# Assessment of a macroscopic model for the aerothermodynamics characterization of Ice Giants atmospheric entry

D. Ninni<sup>1\*</sup>, F. Bonelli<sup>1†</sup>, A. Laricchiuta<sup>2‡</sup>, G. Colonna<sup>2§</sup>, G. Pascazio<sup>1</sup>¶

## 1 Framework

One of the frontiers of the present era of space exploration is represented by missions toward Gas and Ice Giants, that are recognized as essential for science as well as for aerospace industry. In particular, the Ice Giant planets, Uranus and Neptune, represent a relatively unexplored class of planets [1,2]. Several space research missions have been carried out in the last years with the purpose of better understanding the nature of these planets (atmosphere, composition, magnetosphere, gravity field, magnetic field [3]). Many of these missions have concerned Jupiter (Pioneer 10, 11 and Voyager 1, 2 flyby) and Saturn (Cassini-Huygens, Pioneer and Voyager spacecrafts flyby). On the other hand, the only close analysis of Uranus and Neptune comes from the Voyager 2 flyby [3]. Thus, NASA and ESA are currently highly motivated to devise an atmospheric probe mission for Ice Giants [1,4]. Typical velocity and stagnation enthalpy values of atmospheric entry into Uranus or Neptune are 22 km/s and 249 MJ/kg [4], respectively, thus requiring the development of a proper Thermal Protection System (TPS) through the study of the aerothermodynamic environment developing around the probe.

Under these high speed flight conditions, thermochemical non-equilibrium occurs due to the high temperature reached by the mixture across the detached shock wave in front of the body. Moreover, given the high enthalpy regime, internal energy modes are excited (rotational, vibrational and electronic) and dissociation and ionization effects influence the chemical composition, giving rise to free electrons and charged species (atoms or molecules) in the mixture. From the computational point of view, the most common approach to study thermochemical non-equilibrium is the multi-temperature model (mT) [5] considering the

<sup>&</sup>lt;sup>1</sup>Dipartimento di Meccanica, Matematica e Management, Politecnico di Bari, Bari, Italy 
<sup>2</sup>CNR ISTP Bari section, Bari, Italy

<sup>\*</sup>davide.ninni@poliba.it

<sup>†</sup>francesco.bonelli@poliba.it

<sup>&</sup>lt;sup>‡</sup>annarita.laricchiuta@cnr.it

<sup>§</sup>gianpiero.colonna@cnr.it

<sup>¶</sup>giuseppe.pascazio@poliba.it

translational and rotational energy modes in equilibrium at the gas temperature, T, whereas vibrational and electronic modes follow Boltzmann distributions at different temperatures  $(T_{vib} \text{ and } T_e)$ , the latter being commonly considered at equilibrium  $(T_{vib} = T_e = T_{ve})$ . The effects of thermal non-equilibrium on chemical reaction rates are then considered using an effective temperature in the Arrhenius formula, that is a geometrical average of T and  $T_{ve}$ . However, it was recently demonstrated that at hypersonic speeds internal distributions may depart from the Boltzmann one and mT models can introduce considerable errors [6], thus requiring the employment of a detailed State-to-State (StS) approach. It consists in determining the evolution of each internal level, estimating their distribution, without defining an internal temperature, but at the cost of a very demanding kinetics solver.

The aim of this work is to present an hybrid  $\mathrm{mT/StS}$  model for the numerical simulation of Ice Giants hypersonic re-entry. An hydrogen/helium mixture is considered for the flow past a bluff body, where only electronic modes of  $\mathrm{H}_2$  and  $\mathrm{H}$  are treated with a State-to-State approach (namely, only the ground state is considered for the vibrational mode of  $\mathrm{H}_2$ ). This allows for an accurate description of the internal levels, at a reduced computational cost.

# 2 Methodology

## 2.1 Kinetics approach

In last years, the authors have been developing an in-house CFD solver equipped with GPU in order to reduce the computational cost required by the simulations of hypersonic flows with detailed kinetics [7]. The governing equations, written in vectorial form, read:

$$\int_{\mathcal{V}_0} \frac{\partial}{\partial t} \mathbf{U} \, d\mathcal{V} + \oint_{S_0} \mathbf{F} \cdot \mathbf{n} \, dS = \int_{\mathcal{V}_0} \mathbf{W} \, d\mathcal{V} \tag{1}$$

where **U** and **W** are the vector of conservative variables and source terms respectively, whereas  $\mathbf{F} = (\mathbf{F}_{\mathrm{I}}^{x} - \mathbf{F}_{\mathrm{V}}^{x}, \mathbf{F}_{\mathrm{I}}^{y} - \mathbf{F}_{\mathrm{V}}^{y}, \mathbf{F}_{\mathrm{I}}^{z} - \mathbf{F}_{\mathrm{V}}^{z})$  are the fluxes across each control volume's surface; here, subscripts I and V stand for inviscid and viscous fluxes. In the proposed model, the conservative varibale vector reads:

$$\mathbf{U} = \begin{bmatrix} \rho_{\mathrm{H}_{2}(l=0)} \\ \vdots \\ \rho_{\mathrm{H}_{2}(l=4)} \\ \rho_{\mathrm{H}(n=1)} \\ \vdots \\ \rho_{\mathrm{H}(n=4)} \\ \rho_{\mathrm{He}} \\ \rho u \\ \rho v \\ \rho w \\ \rho E \\ \rho_{\mathrm{H}_{2}} \varepsilon_{vib,\mathrm{H}_{2}} \end{bmatrix}$$

$$(2)$$

where (u,v,w) are the Cartesian velocity components, E is the specific total energy of the mixture,  $\rho_{H_2(l)}$  and  $\rho_{H(n)}$  are the partial densities of the generic electronic level of  $H_2$  and  $H_1$ , respectively. In the present kinetic model 5 electronic levels are considered for  $H_2$  and 4 for  $H_1$ , whose characteristics (energy and statistical weight) are reported in tables 1 and 2. Moreover, according to a macroscopic approach, the solver requires a transport equation also for the vibrational energy of  $H_2$  ( $\varepsilon_{vib,H_2}$ ). The corresponding vibrational temperature is properly calculated, relying on the detailed kinetics provided by the StS approach using 15 vibrational levels, thus reducing the computational cost while preserving an accurate description of the thermochemical properties.

Table 1:  $H_2$  electronic level characteristics.

Level	$\varepsilon$ [eV]	g
l = 0  (ground)	0.0	1.0
l = 1	11.1785	1.0
l=2	12.2875	2.0
l=3	13.6921	1.0
l=4	13.9971	2.0

Table 2: H electronic level characteristics.

Level	$\varepsilon$ [eV]	g
n = 1  (ground)	0.0	2.0
n=2	10.1986	8.0
n=3	12.0872	18.0
n=4	12.7482	32.0

The source terms of the electronically excited  $H_2$  partial density equations (l > 0) are evaluated basing on state-specific data [8]. For a consistent macroscopic approach of the vibrational ground state mode of energy, one needs to weight the vibrational state-specific data  $(k_f^v(T))$  on the vibrational Boltzmann distribution  $f_v^B(T_{vib})$ , in order to obtain the macroscopic forward rates  $(k_f(T, T_{vib}))$ . For the generic process

$$H_2(v) + X \rightleftharpoons products$$
 (3)

the macroscopic forward rate is obtained as

$$k_f(T, T_{vib}) = \sum_v k_f^v(T) f_v^B(T_{vib}) \tag{4}$$

with

$$f_v^B = \frac{g_v e^{-\varepsilon_v/k_B T}}{O^v} \tag{5}$$

where  $k_B$  the Boltzmann constant,  $g_v$  and  $\varepsilon_v$  are the statistical weight and energy with respect to the ground state of the level v and

$$Q^{v} = \sum_{v}^{V_{m}} g_{v} e^{-\varepsilon_{v}/k_{B}T} \tag{6}$$

the vibrational partition function ( $V_m = 15$  is the number of vibrational states).

To determine the contribution of such reaction to the vibrational energy, gains  $(\mathcal{G})$  and loss  $(\mathcal{L})$  terms have been added to the Landau-Teller vibrational energy relaxation equation

$$\frac{d\varepsilon_{vib,H_2}}{dt} = \frac{\varepsilon_{vib,H_2}(T) - \varepsilon_{vib,H_2}(T_{vib})}{\tau} + \mathcal{G} - \mathcal{L}$$
(7)

where  $\tau$  is the vibrational energy relaxation time due to vibration-translation (VT) processes and

$$\mathcal{L}(T, T_{vib}) = \sum_{v} \varepsilon_v k_f^v(T) f_v^B(T_{vib})$$
(8)

The corresponding backward rates,  $k_b$ , and  $\mathcal{G}$ , depending only on the gas temperature, are calculated using the detailed balance principle

$$k_b(T) = \frac{k_f(T, T)}{Z_{eq}(T)} \qquad \mathcal{G}(T) = \frac{\mathcal{L}(T, T)}{Z_{eq}(T)} \tag{9}$$

where  $Z_{eq}$  is the generalized equilibrium constant to account for excited species. Writing a reaction in the form

$$\sum_{s} a_s X_s(l_s) = 0 \tag{10}$$

being  $a_s$  the stoichiometric coefficients of species  $X_s$  in the level  $l_s$  (positive for products and negative for reactants), the equilibrium condition reads

$$k_b(T) \prod \left( n_s^{eq}(T) f_{s,l_s}^B(T) \right)^{a_s} = k_f(T,T)$$
(11)

where  $n_s^{eq}$  is the particle density at equilibrium and  $Q_s$  appearing in the Boltzmann distribution  $f_{s,l_s}^B(T)$  is the partition function of species s calculated on the level included in the model. It should be noted that in the hybrid approach, the statistical weight of the ground state of  $H_2$  is given by  $Q^v(T_{vib})$  while its energy is null. Defining

$$\Pi_g = \prod_s g_{s,l_s}^{a_s} \qquad \Pi_\varepsilon = \prod_s e^{-a_s \varepsilon_{s,l_s}/k_B T}$$

$$\Pi_Q = \prod_s Q_s^{a_s} \qquad K_{eq} = \prod_s (n_s^{eq})^{a_s} = \prod_s (Q_s^{ALL})^{a_s}$$

the generalized equilibrium constant is given by

$$Z_{eq}(T) = \frac{\Pi_g K_{eq}}{\Pi_Q \Pi_{\varepsilon}} \tag{12}$$

Note that the equilibrium constants  $K_{eq}$  are evaluated from first principle, considering the "real" thermodynamic functions of reacting species. The mechanisms considered are the following:

$$\begin{split} \mathrm{H_2}(l>0) + \mathrm{H_2} &\leftrightarrow 2\mathrm{H}(n=1) + \mathrm{H_2} \\ \mathrm{H_2}(l>0) + \mathrm{H} &\leftrightarrow 2\mathrm{H}(n=1) + \mathrm{H} \\ \mathrm{H_2}(l>0) + \mathrm{He} &\leftrightarrow 2\mathrm{H}(n=1) + \mathrm{He} \\ \mathrm{H_2}(l=0) + \mathrm{H}(n=2) &\leftrightarrow 3\mathrm{H}(n=1) \\ \mathrm{H_2}(l>0) &\to \mathrm{H_2}(l=0) + h\nu \\ \mathrm{H_2}(l=1) &\to 2\mathrm{H}(n=1) + h\nu \\ \mathrm{H}(n>1) &\to \mathrm{H}(n'< n) + h\nu \end{split}$$

indicating with  $h\nu$  the emission of a photon.

## 2.2 Transport properties

The mixture transport properties are estimated through mixing rules. Single-species first-order coefficients [9], viscosity and thermal conductivity, depend directly on collision integrals of order (2,2), while binary diffusions are derived from diffusion-type collision integrals,  $\Omega_{ij}^{1,1}$ , relevant to the i-j collisional system. The accuracy of properties relies on the use of the database of thermally-averaged transport cross sections, constructed, in the frame of a hybrid approach, for the Jupiter atmosphere [10].

#### 2.3 Numerical scheme

The solver calculates the inviscid fluxes by means of the Steger-Warming flux vector splitting scheme [11], for which a second order accurate MUSCL discretization is used [12]. Diffusive fluxes discretization is performed through a centered, second order accurate scheme. Lastly, in order to exploit GPU capabilities, an explicit, third order accurate Runge-Kutta scheme is employed for time advancement. More in detail, the solution is updated in two steps: in the first one, homogeneous equations are solved (without thermochemistry source terms); in the second step, source terms due to vibrational excitation and chemical activity are evaluated by means of the implicit Gauss-Seidel scheme. This procedure, suitable for reactive flows [13], ensures stability and time-accurate solution with a reasonable time-step size, providing same results as those obtained by using a fully-implicit scheme [14, 15].

## 3 Results

#### 3.1 0D chemical reactor

A preliminary analysis has been carried out to assess the accuracy of the proposed macroscopic approach with respect to StS results. First of all, a constant density 0D reactor is simulated to assess the chemical solver of a neutral hydrogen mixture composed of two species (H<sub>2</sub> and H). The initial conditions are summarized in table 3. Two different thermal conditions are considered, namely thermal equilibrium  $(T = T_{vib})$  and thermal non-equilibrium  $(T \neq T_{vib})$ . Figure 1 shows the temporal evolution of the gas temperature and species mass fractions for the equilibrium case, whereas figure 2 illustrates the results for the thermal non-equilibrium case, reporting also the trend of the vibrational temperature. The initial value of the vibrational temperature for this case is  $T_{vib} = 300 \text{ K}$ .

Table 3: Initial conditions for the 0D chemical reactor.

p [atm]		$\rho \; [\mathrm{kg/m^3}]$	_	
1	6014	$4.032 \times 10^{-3}$	1.0	0.0

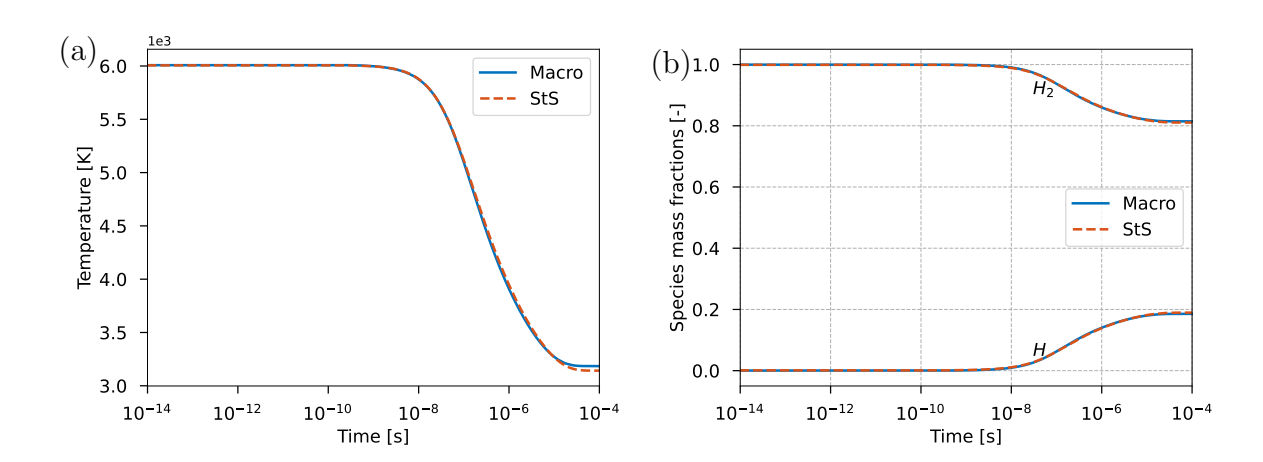


Figure 1: Temperature (a) and species mass fraction (b) profiles for the 0D reactor in thermal equilibrium.

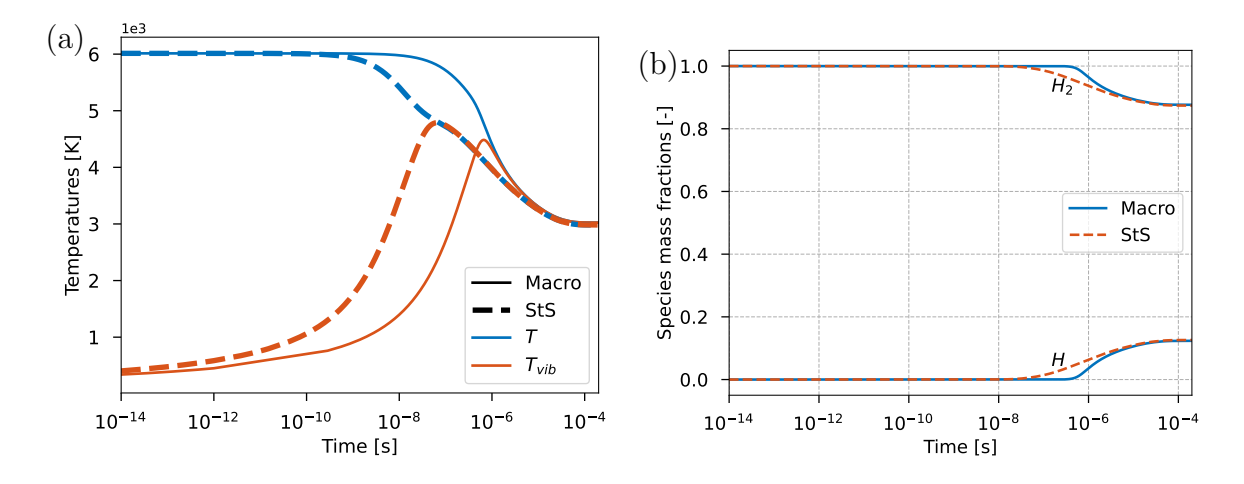


Figure 2: Temperature (a) and species mass fraction (b) profiles for the 0D reactor in thermal non-equilibrium.

The thermal non-equilibrium influences the results leading to a delayed and faster relaxation to the steady state in the case of the macroscopic model. Indeed, also the dissociation of H<sub>2</sub> is delayed and faster, as can be observed by comparing Figure 1(b) and Figure 2(b). However, in both cases a dissociation rate of about 20% is reached at steady state.

## 3.2 Hypersonic flow past Galileo capsule

In order to assess the prediction capability of the proposed macroscopic model, coupled with the fluid dynamics solver, 2D axis-symmetric numerical simulations have been performed. A hypersonic flow past the nose of Galileo capsule, as illustrated in the work by Coelho and Da Silva [16], is taken as reference. Specifically, the '45° Entry' case is simulated. This test represents a benchmark to investigate the main differences between the macroscopic and StS model proposed in this work. The free stream conditions are here summarized:  $p_{\infty} = 892$  Pa,  $M_{\infty} = 33$ ,  $\rho_{\infty} = 4.229 \times 10^{-3}$  kg/m³ (molar composition is 81% H<sub>2</sub> and 19% He). In such flight conditions, ionization is not expected. Hence, the mixture is considered neutral and composed of H<sub>2</sub>, H and He only. No slip and null pressure gradient boundary conditions are imposed at wall, considered inert and at constant temperature ( $T_w = 1000$  K).

Contour maps of gas temperature are shown in Figure 3: the right hand side illustrates the results obtained by means of the macroscopic model, whereas StS results are reported on the left hand side. In order to provide a quantitative comparison, temperature profiles have been extracted along the stagnation streamline. The results are shown in Figure 4, together with literature results obtained by Coelho and Da Silva [16] (referred to as Coelho 2023 in the legend), who performed macroscopic approach simulations. The StS model provides a very similar shock stand-off distance. Moreover, in the relaxation region (plateau) the value of the temperature is in a very good agreement with expectations. It can be also observed that the vibrational temperature profiles are almost overlapped to those of the gas temperature (not reported in the same graph for a better view): this is expected as the molecular hydrogen dissociates very quickly, reaching a very low mass fraction in the shock layer, as shown in Figure 5.

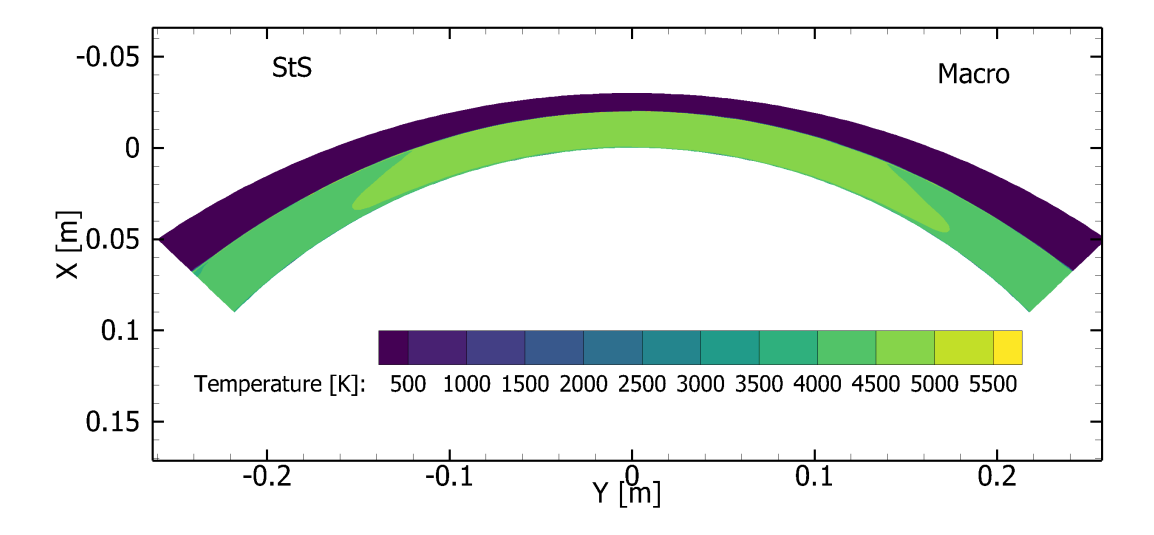


Figure 3: Contour maps of the gas temperature: StS (left) and macroscopic (right) models.

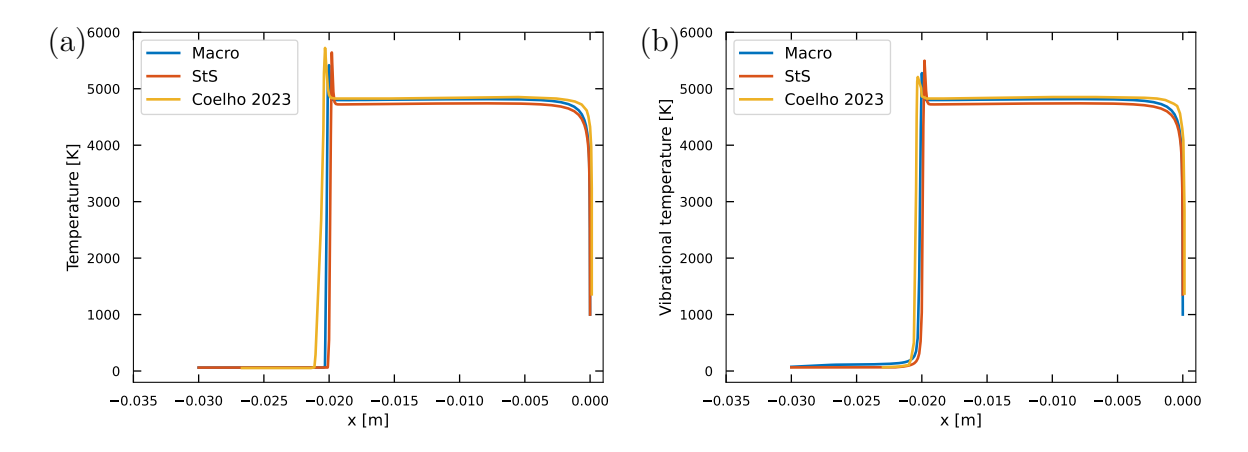


Figure 4: Gas temperature (a) and vibrational temperature (b) profiles along the stagnation streamline.

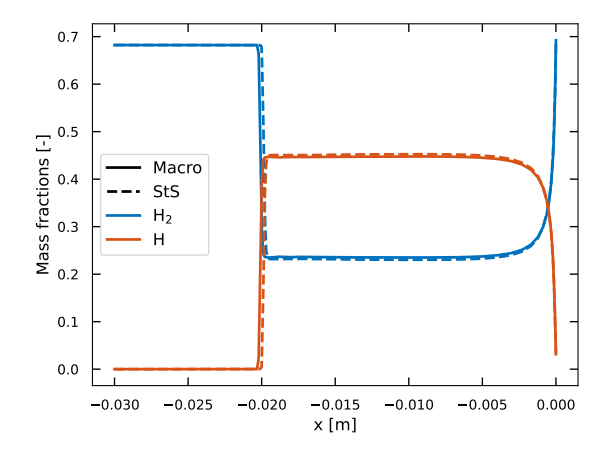


Figure 5: Mass fraction profiles along the stagnation streamline.

# 4 Conclusion and perspectives

This work presents preliminary results obtained by simulating a hypersonic flow past a bluff body for Ice Giant atmospheric entry. Two kinetic models have been compared with each other, namely the state-to-state and the macroscopic models developed at National Research Council in Italy. The two models provide very similar dissociation rates for a 0D reactor case when thermal equilibrium is assumed. On the contrary, thermal non-equilibrium condition leads to slightly different dissociation rates. However, when coupled with the fluid dynamics, these differences are negligible for the presented test case. Specifically, the shock stand-off distance is comparable between the two models, and in good agreement with the numerical solution in the literature.

The simulation presented in this manuscript is characterized by a low free stream enthalpy, not large enough to promote ionization and radiation phenomena. However, the complete models (both StS and mT one) involve also charged species and electron excitation/ionization/radiation processes for  $H_2$  and H. Numerical simulations are ongoing to assess the capability of the solver in the presence of charged species  $(H^+, H^-, H_2^+, H_3^+)$  [17].

# Acknowledgements

This research is granted by the European Space Agency (ESA) under the ESA Contract No. 4000139351/22/NL/MG.

D. Ninni, F. Bonelli and G. Pascazio were partially supported by the Italian Ministry of University and Research under the Programme "Department of Excellence" Legge 232/2016 (Grant No. CUP - D93C23000100001).

# Copyright Statement

The authors confirm that they, and/or their company or organization, hold copyright on all of the original material included in this paper. The authors also confirm that they have obtained permission, from the copyright holder of any third party material included in this paper, to publish it as part of their paper. The authors confirm that they give permission, or have obtained permission from the copyright holder of this paper, for the publication and distribution of this paper as part of the ICAS proceedings or as individual off-prints from the proceedings.

## References

- [1] Mark Hofstadter, Amy Simon, Sushil Atreya, Donald Banfield, Jonathan J Fortney, Alexander Hayes, Matthew Hedman, George Hospodarsky, Kathleen Mandt, Adam Masters, et al. Uranus and Neptune missions: A study in advance of the next Planetary Science Decadal Survey. *Planetary and Space Science*, 177:104680, 2019.
- [2] Leigh N Fletcher, AA Simon, MD Hofstadter, CS Arridge, Ian J Cohen, A Masters, K Mandt, and A Coustenis. Ice giant system exploration in the 2020s: an introduction. *Philosophical transactions of the royal society A*, 378(2187):20190473, 2020.
- [3] Asif A Siddiqi. Beyond Earth: A chronicle of deep space exploration, 1958-2016, volume 4041. National Aeronautis & Space Administration, 2018.
- [4] Joseph Steer, Peter Collen, Alex Glenn, Tamara Sopek, Christopher Hambidge, Luke Doherty, Matthew McGilvray, Stefan Loehle, and Louis Walpot. Experimental simulation of a Galileo sub-scale model at Ice Giant entry conditions in the T6 free-piston driven wind tunnel. 2022.
- [5] Chul Park. Nonequilibrium hypersonic aerothermodynamics. 1989.
- [6] G Colonna, F Bonelli, and G Pascazio. Impact of fundamental molecular kinetics on macroscopic properties of high-enthalpy flows: The case of hypersonic atmospheric entry. *Physical Review Fluids*, 4(3):033404, 2019.
- [7] Giuseppe Pascazio, Davide Ninni, Francesco Bonelli, and Gianpiero Colonna. Hypersonic flows with detailed state-to-state kinetics using a GPU cluster. In *Plasma Modeling* (Second Edition): Methods and applications. IOP Publishing, 2022.

- [8] Gianpiero Colonna, Lucia Daniela Pietanza, and Annarita Laricchiuta. Ionization kinetic model for Hydrogen-Helium atmospheres in hypersonic shock tubes. *International Journal of Heat and Mass Transfer*, 156:119916, 2020.
- [9] Joseph O Hirschfelder, Charles F Curtiss, and R Byron Bird. The molecular theory of gases and liquids. John Wiley & Sons, 1964.
- [10] Domenico Bruno, C Catalfamo, M Capitelli, G Colonna, O De Pascale, P Diomede, C Gorse, A Laricchiuta, Savino Longo, D Giordano, et al. Transport properties of high-temperature Jupiter atmosphere components. *Physics of Plasmas*, 17(11), 2010.
- [11] Joseph L Steger and RF Warming. Flux vector splitting of the inviscid gasdynamic equations with application to finite-difference methods. *Journal of computational physics*, 40(2):263–293, 1981.
- [12] Bram Van Leer. Towards the ultimate conservative difference scheme. V. A second-order sequel to Godunov's method. *Journal of computational Physics*, 32(1):101–136, 1979.
- [13] Jan G Verwer. Gauss–Seidel iteration for stiff ODEs from chemical kinetics. SIAM Journal on Scientific Computing, 15(5):1243–1250, 1994.
- [14] Davide Ninni, Francesco Bonelli, Gianpiero Colonna, and Giuseppe Pascazio. Unsteady behavior and thermochemical non equilibrium effects in hypersonic double-wedge flows. *Acta Astronautica*, 191:178–192, 2022.
- [15] Davide Ninni, Francesco Bonelli, Gianpiero Colonna, and Giuseppe Pascazio. On the influence of non equilibrium in the free stream conditions of high enthalpy oxygen flows around a double-cone. *Acta Astronautica*, 201:247–258, 2022.
- [16] João Coelho and Mário Lino da Silva. Aerothermodynamic analysis of Neptune ballistic entry and aerocapture flows. *Advances in Space Research*, 71(8):3408–3432, 2023.
- [17] Davide Ninni, Francesco Bonelli, Gianpiero Colonna, Annarita Laricchiuta, and Giuseppe Pascazio. Assessment of hybrid Macroscopic/State-to-State model for numerical simulation of Ice Giant orbit insertion. Submitted to the International Journal of Heat and Mass Transfer, 2024.